2020 IEEE International Conference on Robotics and Automation (ICRA)
31 May - 31 August, 2020. Paris, France

A Novel Articulated Soft Robot Capable of Variable Stiffness through Bistable Structure

Yong Zhong, *Member, IEEE,* Ruxu Du, Liao Wu, and Haoyong Yu, *Member, IEEE*

***Abstract*— Soft robot has demonstrated promise in unstructured and dynamic environments due to unique advantages, such as safe interaction, adaptiveness, easy to actuate, and easy fabrication. However, the highly dissipative nature of elastic materials results in small stiffness of soft robot which limits certain functions, such as force transmission, position accuracy, and load capability. In this paper, we present a novel articulated soft robot with variable stiffness. The robot is constructed by rigid joints and compliant bistable structures in series. Each joint can be independently locked through triggering the bistable structure to touch the mechanical constrain. Thus, the bending stiffness of the joint can be magnified which increases the stiffness of the articulated soft robot. Through this construction method, even driven by only one servomotor, the robot demonstrates variable workspace and stiffness which have the potential of dexterous manipulation and maintaining shape under tip load.**

***Index Terms*— Articulated Soft Robot, Variable Stiffness, Bistable Structure, Locking Function**

I. INTRODUCTION

Soft robot, featured by elastic materials and compliant structures, has some unique advantages such as simple structure, safe interaction, adaptiveness, easy to actuate, and easy fabrication [1, 2]. However, these soft robotic systems lost the precision, repeatability, large load capability and stiffness when conducting most industrial tasks, which are the main challenges that limit the extensive applications of soft robots. Lots of scientists and engineers have been attracted to devote into the related research. One of the main challenges is to improve the stiffness of soft robot. Current advances for solving this problem focus on materials stiffening methods and mechanical stiffening methods.

Materials stiffening means change the Young's Modulus of the materials or enable deformation through stimulus. Shape memory effect of shape memory materials has been adopted to exploit the high dexterity in bioinspired robots, such as octopus arms and squid tentacles[3, 4]. A multilayer structure with variable stiffness based on shape memory polymer (SMP) has been presented in [5], the beam is composed of two rigid layers, with a polymer in between. Depending on the polymer state, the entire multilayered beam presents high or low flexural stiffness. Another similar approach depends on segmented materials combined with the variable-stiffness SMP matrix material[6], and it successfully extends the stiffness variation range up to 77 times. Dielectric elastomer, another type of material suitable for electrically activated soft robots, also be exploited the ability to vary stiffness [7]. Low melting point materials and glass transition-based softening also have been integrated in soft robots to vary stiffness[8, 9] [10]. Cheng et al. [11] has presented an approach that coating wax on flexible open cells demonstrates large stiffness-changing range, and has been applied on locking joint systems or shape-shifting structures. To obtain higher stiffness variation, low melting point alloy (LMPA) is required in soft robot. Such as LMPA embedded in soft polydimethylsiloxane，[12] demonstrates a relative stiffness change higher than 25 times and a fast transition from rigid to soft states. Other approaches include using megneto-and electrorheological materials, such as magnetorheological fluids (MRFs), MR elastomers, electrorheological (ER) fluids, and ER elastomers, and hybrid multimaterial 3D printing. Combining with soft materials, the same principal can be exploited to increase the stiffness of soft structures [13-16]. In summary, materials stiffening methods have advantages for varying stiffness of soft robots, but they also suffer some problems such as encapsulation difficulty, integration, fabrication, and energy inefficient. Moreover, they cannot be changed to be large stiffness, thus, the deployment in real applications is limited.

Mechanical stiffening methods are also exploited for variable stiffness in soft robots. For example, soft pneumatic actuators with embedded sheet, fiber structures or folded structures have been developed to increase the stiffness and anisotropy of the elastomeric actuators [17, 18]. Fluid driven robotic system with origami structure has demonstrated large load capability, and flexible arm with the vacuum driven joints also demonstrated reliable stiffness [19, 20]. Jamming technology was also utilized to build soft robots, through sucking the air or liquid between the granular medium in the robots, the stiffness can be changed to modulate the direction and magnitude of the performance [21, 22]. These approach all need continuous energy supply and suffer seal and leak problems. Utilizing pure mechanical mechanisms can also enable the variable stiffness for soft robots. For example, Howie Choset et al. [23] presented a snake robot for minimal invasive surgery. Similar approach has been proposed by Zheng Li et al. [24] and Shuxin Wang et al. [25] that using telescopic tube or spine to constrain the flexibility of soft robot resulting in stiffness change. Though the mechanical mechanisms approaches suffer some problem, such as the mechanical complexity, weight and size, these approaches can offer quite large stiffness through mechanical constrains, and can be easily implemented in real applications.

Research was supported by the Strategic Priority Research Program of the Chinese Academy of Sciences (class A) (Grant No. XDA22040203), and the Fundamental Research Funds for the Central Universities (Grant No. 2019XX01).

Yong Zhong and Ruxu Du are with Shien-Ming Wu School of Intelligent Engineering, South China University of Technology, Guangzhou, China (email: zhongyong@scut.edu.cn, duruxu@scut.edu.cn).

Liao Wu is with School of Mechanical and Manufacturing Engineering, Faculty of Engineering, University of New South Wales, Sydney NSW 2052 Australia (e-mail: liao.wu@unsw.edu.au).

Haoyong Yu is with Department of Biomedical Engineering, National University of Singapore, Singapore 119077 (e-mail:,bieyhy@nus.edu.sg).

In this paper, we exploited the mechanical mechanism approach to change stiffness for soft robot. we proposed a novel articulated soft robot with variable stiffness and workspace. It consists of 7 articulated joint, and each joint has a pair of bistable structures. The whole robot is driven by only one servomotor through cables as our previous work [26]. The stiffness change is achieved through locking function of each joint. The locking function is implemented by triggering bistable structure between each joint. Each bistable structure is triggered by a pair of shape memory alloy springs. Thus, each joint can be independently controlled to be locked, and the stiffness is then magnified by pure mechanical constrain. Through locking selected joints, the robot demonstrates variable workspace and stiffness. With these new properties, we envision broader applications of this articulated soft robot. Section II introduces the design and prototype of the novel articulated soft robot. Section III illustrates the kinematics, workspace, stiffness evaluation metric, and dexterity analysis of the robot. Section IV gives the experimental results of the actuation, joint locking function, and thermal view of the robot. Finally, in Section V, we give the conclusions, limitations, and future work.

II. Robot Design and Implementation

Articulated soft robots are robots with both soft and rigid parts that inspired by the muscle-skeletal system of vertebrate animals – from reptiles to birds to mammalians to humans. Compliance is typically concentrated in actuators, transmission and joints while structural stability is provided by rigid or semi-rigid links. In this section, we present the design and implementation of a new type of articulated soft robot utilizing bistable structures, and briefly introduce the actuation principal of the bistable structures.

A. Bistable structure actuation

Bistable actuation is commonly found in biological systems, such as the Venus fly trap [27] and the Mantis shrimp [28] which rely on this type of actuation to prey and defense. Bistable structure is one that has three mechanical stats: two stable states and one instable state, and the switch between them only needs a small trigger force [29, 30]. It is a good method to maintain status of the robotic system without continuous power supply and also an amplifying mechanism to transmit displacement and force.

Here, we illustrate a conceptual design to show the actuation principals of bistable structures in an articulated joint. The bistable structure is designed similar to a flexible hinge where the neck and waist parts are easy to deform (Fig. 1A), and is installed in both sides of a pin joint. The main parameters of bistable structure are neck length (l_0), beam length (l_1), beam width (w), and waist length (l_2). Since the thickness of the bistable structure does not affect the geometric relationship of the joint, we don't address it here. The joint with bistable structures has three modes: free bending, right locking, and left locking (Fig. 1B, C, and D). When it is in free bending mode, the potential energy of the deformation of the bistable structures supplies the recovery force for the joint, which metamorphosing the joint into a type of elastic joint with compliance and adaptiveness. When the locking function is needed, the joint first rotates to an angle larger than the locking angle, then using external force to trigger the bistable structure to transit from outward bending to inward bending (i.e. one stable state to another stable state shown in Fig. 1C). Next, the structure would touch the joint pin forming a mechanical constrain, and the joint would be locked in the locking direction. This physical locking mode can hugely magnify the bending stiffness of the joint. When it needs to recover to the free bending mode, it just need to bend the joint to limit bending angle on the unlocking direction, then retract the joint in the locking direction, the bistable structure would recover to outward bending relying on the protential energy of neck deformation.

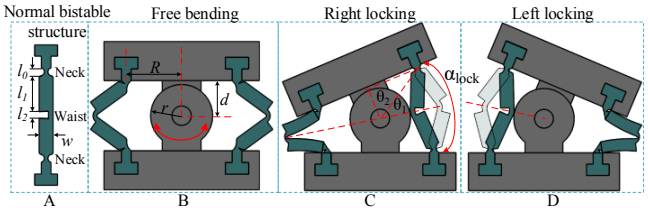

Fig. 1. Example of bistable structures in an articulated joint.

The locking angle is determined by the dimensional parameters of both the joint and the bistable structure, and can be mechanically preprogrammed by modularly designing different bistable structures. An estimated calculation of locking angle based on geometric relationship is given by

$$\alpha_{lock} = 2(\theta_1 + \theta_2 - 90°), \quad (1)$$

where

$$\theta_1 = \cos^{-1}\frac{R^2+(d-l_0/2)^2+\left(r+w/(2\sin(\tan^{-1}(2w/l_2)))\right)^2-(l_0/2+l_1+l_2/4)^2}{2\sqrt{R^2+(d-l_0/2)^2}\left(r+w/(2\sin(\tan^{-1}(2w/l_2)))\right)}$$

and $\theta_2 = \cos^{-1}\frac{d-l_0/2}{\sqrt{R^2+(d-l_0/2)^2}}$.

B. Articulated Soft Robot Design and Implementation

Based on the actuation principal of an articulated joint with bistable structure shown in Fig. 1, we proposed an articulated soft robot arm. This robot is just to show our concept, thus, it is designed to be simple and only conducts planar motion. The robot consists of 7 articulated joints (Fig. 2A), and each joint installs a pair of bistable structures on both sides. The whole robot is driven by only one servomotor through steel cables, and the cables go across all the joint links in an underactuation way. The servomotor is to control the motion and shape of the robot arm, and each joint can be independently controlled to locking modes through triggering the modes transition of the bistable structures. The prototype of the joint in Fig. 2B shows that the bistable structures are triggered by shape memory alloy (SMA) springs. Here, a type of SMA spring with a transition temperature of 45˚C is adopted to trigger the structure. Through electric power, the SMA springs are heated to recover to the memorized shape generating tensile forces. The forces pull the bistable structures to the locking modes (Fig. 2C). The parameters of the bistable structure in this paper are: l_0=2mm, l_1=9mm, w=3.6mm, and l_2=2mm, respectively.

The locking function activation of the joints during the motor driven of the robot arm is similar to single joint actuation principal shown in Fig. 1. The procedure is as follows:

Step 1, driving the robot arm to bend an angle θ_L ($\theta_L \geq N\alpha_{lock}$, N is the number of joints);

Step 2, selecting the joints need to be locked in the locking direction;

Step 3, activating the SMA springs on the selected joints to trigger the locking modes;

Step 4, bending the robot arm to the opposite angle θ_R ($\theta_R \geq [(N\text{-}N_L)\ \alpha_{lock}\text{-}\ N_L\alpha_{lock}]$, N_L is the number of selected joints to be locked);

Step 5, activating the SMA springs on the current selected joints to trigger the locking modes.

This process will be demonstrated in the experiments.

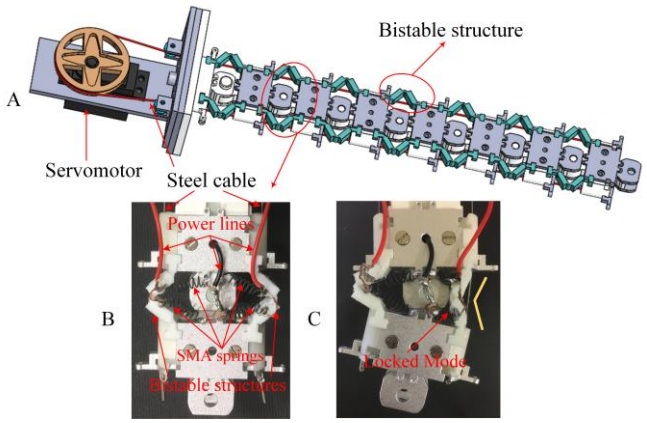

Fig. 2. (A) 3D model illustration of the articulated soft robot arm. (B) A prototype of the joint. (C) The joint is locked.

III. Modeling and Analysis of The Robot

In this section, the kinematics of the articulated soft robot combining the locking function of the joint is presented. The workspace of the new robot, and the stiffness evalutation metric are also illustrated. The dexterity analysis based on dexterity solid angle concept is shown to demonstrate the properties of our robot.

A. Kinematics and Workspace

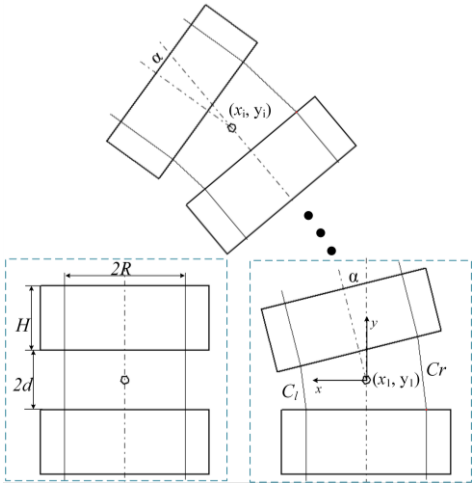

Fig. 3. brief sketch of the joint cable-driven motion.

The kinematics of the cable-driven articulated robot arm can be derived based on the geometric relationship. The bistable structures act as the elastic element of the robot arm which ensure each joint approximately bends uniformly. The brief sketch of the joint can be illustrated as Fig. 3. The length changes of the cables on both sides can reflect bending angle of the joint, and are given by

$$\begin{cases} \Delta C_l = -\left[2R\sin\dfrac{\alpha}{2} + 4d\sin^2\dfrac{\alpha}{4}\right] \\ \Delta C_r = 2R\sin\dfrac{\alpha}{2} - 4d\sin^2\dfrac{\alpha}{4} \end{cases}, \tag{2}$$

where H is the length of the joint link, d is the distance between rotation center and joint, $2R$ is the distance between the parallel cables, α is the bending angle of the joint, C_l and C_r are the lengths of the cables between the joint after bending.

Since each joint is enabled locking function and has three modes, the robot would exhibit numbers of different configurations. We set 0, 1, -1 representing the modes, free bending, left locking, and right locking, respectively. Then the robot would perform N^3 configurations through selectively locking joints, where N is the number of joints. Defining a configuration matrix $M = [m_1\ m_2\ \ldots\ m_i]$, where $i = 1, 2, \ldots N$, and $m_i \in \{-1, 0, 1\}$, then, the forward kinematics can be derived as

$$\begin{cases} x_{i+1}(t) \\ = x_i(t) + (H+2d)\cos\left(\sum_{i=1}^{N}\left(m_i\alpha_{lock} + (1-|m_i|)\alpha_i(t)\right)\right) \\ y_{i+1}(t) \\ = y_i(t) + (H+2d)\sin\left(\sum_{i=1}^{N}\left(m_i\alpha_{lock} + (1-|m_i|)\alpha_i(t)\right)\right) \end{cases} \tag{3}$$

Based on the configuration matrix, we can derive all different configurations of the robot. For the robot in this paper, it has 7 joint which means total $3^7 = 2187$ different configurations. Several different types of configurations enumerated in Fig. 4. Each configuration matrix corresponds to the robot configuration in the picture. *The idealization conditions in this kinematic model are that when one joint is locked, is cannot bending in both directions due to the counter force of opposite bistable structure and the locking function.* However, in the deployment of prototype, the locked joint can still bend in the unlocked direction with small amplitude. Because the counter force from the opposite bistable structure is not enough to withstand the friction and moment generated by the cables. In Fig. 4, the parameters of the robot for the simulation are listed in Table I. Note that with different configuration, the selected joints to be locked are different, and the stiffness and workspace of the robot are also changed. If all joints are locked, the robot can bear tip load depending on the structures themselves.

Table 1. Parameters of the robot

Parameters	Values
Joint limit bending angle α_{limit}	25°
Joint length ($H + 2d$)	38 mm
Locking angle α_{lock}	15°
Cable distance $2R$	40 mm
Joint gap $2d$	18 mm

For each configuration, the tip point of the robot corresponds to the end effector, thus, the trajectory of the tip point denotes the workspace of the end effector. For one segment underactuated cable-driven robot arm without locking function, the workspace is a fix trajectory; for our robot, which enables the joint locking function (LF), it can

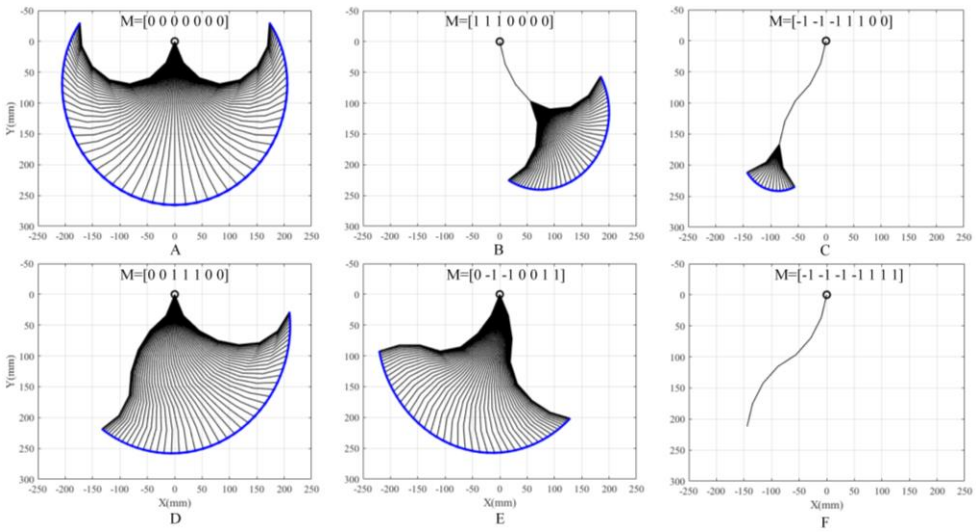

Fig. 4. One example for each type of configuration of cable-driven articulated soft robot. (A) Free bending. (B) Start one-side locking. (C) Start two-side locking. (D) Non-start one-side locking. (E) Non-start two-side locking. (F) Full locking.

demonstrate much larger workspace as shown in Fig. 5. The locked joints increase the local stiffness of the robot which enable the robot to execute more dexterous tasks like that shown in Fig. 4B and C.

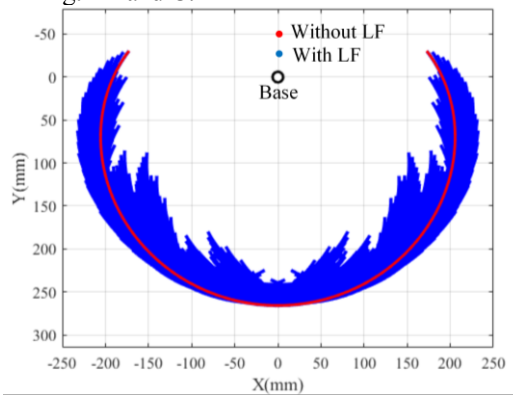

Fig. 5. Comparison of workspace between robot arm with locking function (blue area) and that without locking function (red curve). The resolution for this workspace is 500×500.

B. *Stiffness Evaluation Metric*

The stiffness change in our design is based on the mode's transition of the bistable structure in each joint, thus, it is an on-off change (not continuous). The magnitude of stiffness is determined both by the selected materials and parameters of the bistable structure, and the driving cables of the joint. *However, when we using this type of articulated robot arm in locking status, the cables normally don't bear load in the locking direction, it is the bistable structure that can support the load of the arm without the cables.* The high stiffness mode of the joint is totally determined by the materials selected and the design parameters of the bistable structure. Here, we propose a stiffness evaluation metric for this featured approach.

We assume the designed bending stiffness in the locking direction of each joint is E_L which is determined by the materials and design parameters of the bistable structure, then the stiffness factors refer to joint status in the locking direction are separately set as: High (f_h), Medium (f_m), and Low (f_l). As it is listed in Table 2, if the joint mode is 1 (left locking), the stiffness for bending to left is High, but the stiffness bending to right is Medium due to the counter force of opposite bistable structure in the joint; and if the joint mode is 0, the stiffness for both side is Low. For the robot arm constructed by this type of joints, the stiffness for load capability of each joint, for instant, joint i, is influenced by all the joints from 1 to i. We call it accumulated stiffness (AS).

Table 2. Stiffness Evaluation Table

Joint	mode	stiffness	
		left	Right
1	-1	Medium	High
	0	Low	Low
	1	High	Medium
…	…	…	
i	-1	Medium	High
	0	Low	Low
	1	High	Medium
Accumulated Stiffness		S_{Li}	S_{Ri}

The stiffness factors for bending to left is

$$f_{Li} = \begin{cases} f_h, \ if \ m_i = 1 \\ f_m, \ if \ m_i = -1, \\ f_l, \ if \ m_i = 0 \end{cases} \quad (4)$$

and the AS of joint i for bending to left is

$$S_{Li} = \prod_{j=1}^{i} f_{Lj} E_L \ . \quad (5)$$

The stiffness factors for bending to right is

$$f_{Ri} = \begin{cases} f_m, \ if \ m_i = 1 \\ f_h, \ if \ m_i = -1, \\ f_l, \ if \ m_i = 0 \end{cases} \quad (6)$$

and the AS of joint i for bending to right is

$$S_{Ri} = \prod_{j=1}^{i} f_{Rj} E_L \ . \quad (7)$$

where $M = [m_1 m_2 \ ... \ m_i]$ is the configuration matrix from joint 1 to i. The stiffness factors can be obtained by experiments. Normally, we have $f_h \rightarrow 1^-$, $0 < f_m < 1$, and $0 < f_l < f_m$.

These rules can be taken as the stiffness evaluation metric for measuring the joint stiffness of the articulated soft robot arm under different configuration matrix.

C. Dexterity Analysis

The dexterity of the robot arm is a measure to achieve different orientations for each point within the workspace. It can be measured in several ways, such as by the condition number of the Jacobian matrix [31] and by the product of the singular values [32]. However, these metrics gives little intuitive information. A more intuitive way is to use the absolute kinematic flexibility [33], which is defined as the number of configurations that the manipulator can reach the target.

In this study, the dexterity analysis is based on the dexterity solid angle concept [34]. For an arbitrary point x in the workspace, the robot arm would reach x in more than one configuration. Defining a unit sphere with x as its center, namely the service sphere. The points intersect the service sphere when the robot arm reach the arbitrary point with different orientations form a service region. The dexterous solid angle, $D(x)$, is defined as the ratio of the total area of the service regions, $A_R(x)$, to the area of the service sphere, A_S, at the point x of the end-effector

$$D(x) = \frac{A_R(x)}{A_S} = \frac{N_O(x)}{N_P N_Q} \in (0, 1] \tag{8}$$

where $A_R(x)$ is the area of the service regions at point x and A_S is the total surface area of the unit sphere. As in this paper, we will use a discretization method to obtain the dexterity indices, the surface of the unit sphere is discretized into $N_P \times N_Q$ equal area patches in latitude and longitude. Letting $N_O(x)$ represent the number of orientable patches, the dexterity $D(x)$ equals to $N_O(x)$ divided by $N_P N_Q$. To express the workspace in discretized way, we use Monte-Carlo method to calculate the workspace, that is, randomly sample the joint space, calculate the forward kinematics, and statistically analyze all the reachable positions. By evenly discretizing the plane into patches with side lengths of δx and δy, the workspace can be calculated by

$$W = \int_{x \in W} dx = N_K \delta x \delta y \tag{9}$$

where N_K is the number of reachable patches. Then, the total dexterity over the workspace is defined as

$$D_T = \int_{x \in W} \frac{D(x)}{W} dx = \frac{\sum_{i=1}^{N_K} N_K^i}{N_K N_P N_Q} \tag{10}$$

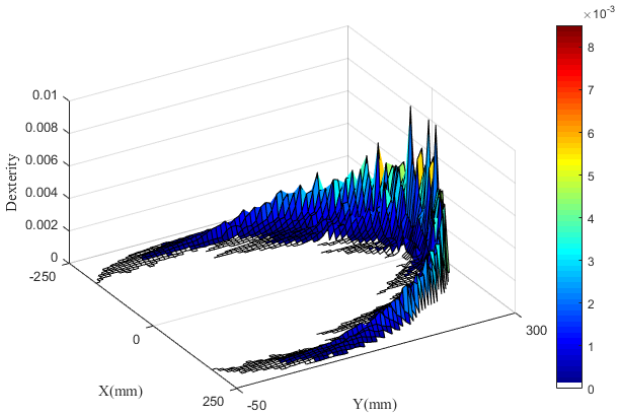

Fig. 6. Dexterity distribution in workspace. The color indicates the dexterity at each position patch.

In the simulation, we randomly collect 2187000 samples from the variation of the joint angle and configurations. The discretization of position is set as $\delta x = \delta y = 5$ mm, and for orientation, we set $N_P = 80$ and $N_Q = 40$. The kinematic model in (3) is used to calculate all the positions of the tip in each configuration. The configuration matrix is randomly generated unrepeatably before simulation loop. All the reachable positions are plotted in a 3D scatter diagram to show the workspace and a color bar is used to indicate the dexterity distribution within the workspace (Fig. 6).

From Fig. 6, we can observe that the total dexterity distribution in the workspace is not that uniform and the dexterity increases with the increase of y axis and reaches the maximum values 0.0079 (i.e. the bottom area in Fig. 5).

IV. Deployment and Experiments

In this section, the hardware architecture is first introduced, and then, the experiments for triggering locking function of joints are presented combining the visualization of thermal imager. Several different configurations are demonstrated, and a tip load test is also presented to show the capability of keep position and shape, even the cable is broken.

A. Deployment of the Robot System

The robot arm is driven by a servomotor (Hitec 7980TH) through steel cables, and the bistable structures are connected to each corresponding joint through a pair of SMA springs (Kellogg's Research Labs). The SMA springs are further connected to a DC power under 5 V (Topward 6306D DC power supply). The SMA springs are activated by the drive modules (BTN7971, a motor drive module which enable large current) controlled by a micro-controller (Arduino mega2560). The SMA activating time is significant, if activated time is too long, the temperature would be too high which would break the shape memory effect. Thus, we use a thermal imager (Optris PI) to visualize the temperature variation and give the feedback to the controller to control the activation of the SMA springs. Most of the components of the articulated soft robot arm are fabricated through 3D printing and CNC machining, and the bistable structures are directly 3D printed by Ultimaker S5 using soft materials (TPU 95A). The parameters for this prototype are the same shown in the previous simulations.

B. Locking Function Demonstration

The locking function of the joints determine the configurations and stiffness of the robot. Figure 7 shows several examples of different configurations of the robot, including start one-side locking (Fig. 7A), start two-side locking (Fig. 7B), and full locking (Fig. 7C). The yellow broken lines indicate the locking directions. The robot arm demonstrates the similar workspace as the simulation results. The stiffness factors in this study are set as f_h =0.99, f_m =0.4, and f_l =0.1 based on our tests. From the stiffness evaluation metric (5) and (7), the tip stiffness of these configurations are $S_{L7} = 2.56e^{-5}\ E_L$, $S_{R7} = 9.6e^{-4}\ E_L$ for Fig. 9A; $S_{L7} = 1.55e^{-3}\ E_L$, $S_{R7} = 6.3e^{-4}\ E_L$ for Fig. 9B; and $S_{L7} = 2.62e^{-4}\ E_L$, $S_{R7} = 9.1e^{-1}\ E_L$ for Fig. 7C. We can see that the tip stiffness for bending to right is much bigger than others. In Fig. 7C, we also have snipped the cable on the right side, it can still bear 0.5kg tip load based on the locking function (no energy is required at this moment), and maintain the shape and keep safe based on the joint stiffness. This property shows the promise to execute

tasks that need payload and manipulation on the end effector of robot with absolute safety.

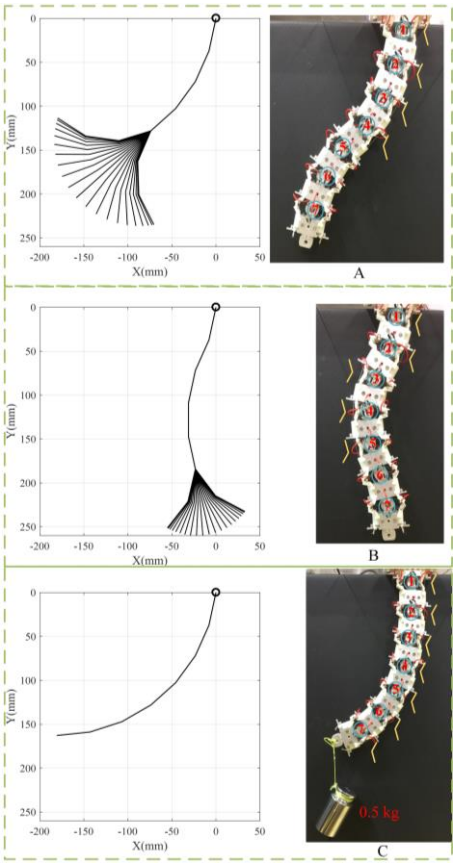

Fig. 7. The demonstration of articulated soft robot arm. (A) Right locking: joint 1 to joint 4, free bending: joint 5 to joint 7. (B) Right locking: joint 1 and joint 2; left locking: joint 3, joint 4, and joint 5; free bending: joint 6 and joint 7. (C) Full locking on the right side.

Since the locking function is achieved by triggering the bistable structure to transit between two stable states, the robot first needs to meet the bistable actuation requirements mentioned in Section II. An example is depicted in Fig. 8, with the visualization of the thermal imager, the process can be explained as follows: first, to right lock the first three joints, the robot bends to the left; second, activating the corresponding SMA springs and deactivating them after locking; third, to lock rest joints on the left, the robot need to bend to the right; Finally, activating the corresponding SMA springs on the rest joints and deactivating them after locking, the robot arm is then fully locked. When the SMA Springs are heated above 45°C (transition temperature), the controller will enable the activation of the SMA springs for 5 seconds to ensure that the bistable structures have been triggered to be locked, and at the same time keep the temperature below 100°C to avoid broken the shape memory effect of the SMA springs through impulse activation. The unlocking process utilizes the potential energy of deformation of the bistable structure to recover. The original bistable structure is design to be straight, thus, the potential energy always tends to recover the deformed structure to be straight. We just need to continuously bend the joint to the locking direction and release it, the bistable structure will be deformed outward and unlock the joint.

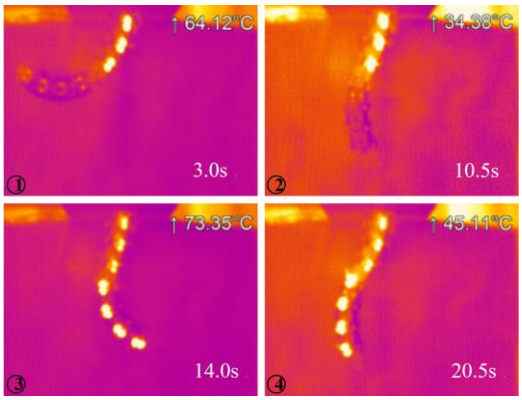

Fig. 8. Thermal view of the locking process of the robot arm. ①→② shows right locking mode of joint 1-joint 3, and ③→④ shows left locking mode of joint 4-joint 7.

V. Conclusion

To tackle one of the main challenges in soft robotics: variable stiffness, we have proposed a new concept to change the stiffness of an articulated soft robot. The variable stiffness is achieved through the locking function of each joint. It is mechanical stiffening method which utilizes the bistable structure and bistable actuation. The bistable structure have the property of two stable states and maintaining the stable states without continuous energy supply. Thus, our robot also owns this advantage that when the joints are locked, they can keep the shape without actuation the servomotor; even the cables are broken, it can still sustain when it is fully locked.

This preliminary study just offers a new vision of how to change the stiffness of soft robot, and it still has some limitations. For example, the locking angle is mechanically preprogrammed by the parameters of bistable structures and it cannot be locked at random angle. Even one can replace different bistable structure and install multi-pairs of bistable structure on the joints to achieve multi-angles locking, it is still not very convenient and efficient in real-time tasks. One drawback of this design is that it requires the whole structure to fully bend and only then you can lock those angles. The SMA trigger methods for the bistable actuation is just one option, one can choose other methods to actuate the bistable structure, such as cable drive, magnet force, and micro motor. The current version of the robot can only conduct planar motion which limits its workspace and dexterity. But, one can connect multiple segments of this articulated soft robot arm in series to enable 3D motion, then, the robot would be capable of more complex tasks.

Our future work will go on improving this design concept for variable-stiffness soft robot, including investigating bistable actuation force and energy, optimizing the design of the robot, and developing control algorithm for real applications.

References

[1] D. Rus and M. T. Tolley, "Design, fabrication and control of soft robots," *Nature,* vol. 521, no. 7553, p. 467, 2015.

[2] C. Laschi, B. Mazzolai, and M. Cianchetti, "Soft robotics: Technologies and systems pushing the boundaries of robot abilities," *Sci. Robot.,* vol. 1, no. 1, p. eaah3690, 2016.

[3] M. Cianchetti, A. Licofonte, M. Follador, F. Rogai, and C. Laschi, "Bioinspired soft actuation system using shape memory alloys," in *Actuators*, 2014, vol. 3, no. 3, pp. 226-244: Multidisciplinary Digital Publishing Institute.

[4] C. Laschi, M. Cianchetti, B. Mazzolai, L. Margheri, M. Follador, and P. Dario, "Soft robot arm inspired by the octopus," *Advanced Robotics,* vol. 26, no. 7, pp. 709-727, 2012.

[5] F. Gandhi and S. G. Kang, "Beams with controllable flexural stiffness," *Smart Materials & Structures,* vol. 16, no. 4, p. 1179, 2007.

[6] G. Mcknight, R. Doty, A. Keefe, G. Herrera, and C. Henry, "Segmented reinforcement variable stiffness materials for reconfigurable surfaces," *Journal of Intelligent Material Systems and Structures,* vol. 21, no. 17, pp. 1783-1793, 2010.

[7] F. Carpi, G. Frediani, C. Gerboni, J. Gemignani, and D. De Rossi, "Enabling variable-stiffness hand rehabilitation orthoses with dielectric elastomer transducers," *Medical engineering & physics,* vol. 36, no. 2, pp. 205-211, 2014.

[8] J. R. Capadona, S. Kadhiravan, D. J. Tyler, S. J. Rowan, and W. Christoph, "Stimuli-responsive polymer nanocomposites inspired by the sea cucumber dermis," *Science,* vol. 319, no. 5868, pp. 1370-1374, 2008.

[9] A. Balasubramanian, M. Standish, and C. J. Bettinger, "Microfluidic Thermally Activated Materials for Rapid Control of Macroscopic Compliance," *Advanced Functional Materials,* vol. 24, no. 30, pp. 4860-4866, 2014.

[10] M. A. Mcevoy and N. Correll, "Thermoplastic variable stiffness composites with embedded, networked sensing, actuation, and control," *Journal of Composite Materials,* vol. 49, no. 15, pp. 1799-1808, 2014.

[11] N. G. Cheng, A. Gopinath, L. Wang, K. Iagnemma, and A. E. Hosoi, "Thermally Tunable, Self-Healing Composites for Soft Robotic Applications," *Macromolecular Materials & Engineering,* vol. 299, no. 11, pp. 1279-1284, 2015.

[12] B. E. Schubert and D. Floreano, "Variable stiffness material based on rigid low-melting-point-alloy microstructures embedded in soft poly(dimethylsiloxane) (PDMS)," *Rsc Advances,* vol. 3, no. 46, pp. 24671-24679, 2013.

[13] C. Majidi and R. J. Wood, "Tunable elastic stiffness with microconfined magnetorheological domains at low magnetic field," *Applied Physics Letters,* vol. 97, no. 16, p. 164104, 2010.

[14] V. Laraprieto, R. Parkin, M. Jackson, V. Silberschmidt, and Z. Kęsy, "Vibration characteristics of MR cantilever sandwich beams: experimental study," *Smart Materials & Structures,* vol. 19, no. 1, p. 015005, 2010.

[15] B. Liu, S. A. Boggs, and M. T. Shaw, "Electrorheological properties of anisotropically filled elastomers," *Dielectrics & Electrical Insulation IEEE Transactions on,* vol. 8, no. 2, pp. 173-181, 2001.

[16] Y. F. Zhang *et al.*, "Fast‐Response, Stiffness‐Tunable Soft Actuator by Hybrid Multimaterial 3D Printing," *Advanced Functional Materials,* vol. 29, no. 15, p. 1806698, 2019.

[17] L. Paez, G. Agarwal, and J. Paik, "Design and analysis of a soft pneumatic actuator with origami shell reinforcement," *Soft Robotics,* vol. 3, no. 3, pp. 109-119, 2016.

[18] A. Rafsanjani, Y. Zhang, B. Liu, S. M. Rubinstein, and K. Bertoldi, "Kirigami skins make a simple soft actuator crawl," *Science Robotics,* vol. 3, no. 15, p. eaar7555, 2018.

[19] S. Li, D. M. Vogt, D. Rus, and R. J. Wood, "Fluid-driven origami-inspired artificial muscles," *Proceedings of the National Academy of Sciences,* p. 201713450, 2017.

[20] M. A. Robertson and J. Paik, "New soft robots really suck: Vacuum-powered systems empower diverse capabilities," *Science Robotics,* vol. 2, no. 9, p. eaan6357, 2017.

[21] J. R. Amend, E. Brown, N. Rodenberg, H. M. Jaeger, and H. Lipson, "A positive pressure universal gripper based on the jamming of granular material," *IEEE Transactions on Robotics,* vol. 28, no. 2, pp. 341-350, 2012.

[22] Y. Wei *et al.*, "A novel, variable stiffness robotic gripper based on integrated soft actuating and particle jamming," *Soft Robotics,* vol. 3, no. 3, pp. 134-143, 2016.

[23] A. Degani, H. Choset, A. Wolf, and M. A. Zenati, "Highly articulated robotic probe for minimally invasive surgery," in *Robotics and Automation, 2006. ICRA 2006. Proceedings 2006 IEEE International Conference on*, 2006, pp. 4167-4172: IEEE.

[24] Z. Li, H. Ren, P. W. Y. Chiu, R. Du, and H. Yu, "A novel constrained wire-driven flexible mechanism and its kinematic analysis," *Mechanism and Machine Theory,* vol. 95, pp. 59-75, 2016.

[25] L. L. CHEN Yuyu, LI Bo, WEI Chao, WANG Shuxin, LI Dichen, "Design, Fabrication and Performance of a Flexible Minimally Invasive Surgery Manipulator Integrated with Soft Actuation and Variable Stiffness," *Journal of Mechanical Engineering,* vol. 54, no. 17, pp. 53-61, 2018.

[26] Y. Zhong, Z. Li, and R. Du, "A Novel Robot Fish with Wire-driven Active Body and Compliant Tail," *IEEE/ASME Transactions on Mechatronics,* 2017.

[27] Y. Forterre, J. M. Skotheim, J. Dumais, and L. Mahadevan, "How the Venus flytrap snaps," *Nature,* vol. 433, no. 7024, p. 421, 2005.

[28] S. Patek, W. Korff, and R. Caldwell, "Biomechanics: deadly strike mechanism of a mantis shrimp," *Nature,* vol. 428, no. 6985, p. 819, 2004.

[29] J. R. Raney, N. Nadkarni, C. Daraio, D. M. Kochmann, J. A. Lewis, and K. Bertoldi, "Stable propagation of mechanical signals in soft media using stored elastic energy," *Proceedings of the National Academy of Sciences,* vol. 113, no. 35, pp. 9722-9727, 2016.

[30] Q. Xu, "Design of a large-stroke bistable mechanism for the application in constant-force micropositioning stage," *Journal of Mechanisms and Robotics,* vol. 9, no. 1, p. 011006, 2017.

[31] J. K. Salisbury and J. J. Craig, "Articulated hands: Force control and kinematic issues," *The International journal of Robotics research,* vol. 1, no. 1, pp. 4-17, 1982.

[32] T. Yoshikawa, "Manipulability of robotic mechanisms," *The international journal of Robotics Research,* vol. 4, no. 2, pp. 3-9, 1985.

[33] J. Lenarcic, Bajd, Tadej, Stanišić, Michael M. , *Robot Mechanisms*. Springer, Dordrecht, New York, 2013.

[34] M. Badescu and C. Mavroidis, "New performance indices and workspace analysis of reconfigurable hyper-redundant robotic arms," *The International Journal of Robotics Research,* vol. 23, no. 6, pp. 643-659, 2004.